PLOS ONE

RESEARCH ARTICLE

Synthesis and Behavior of Cetyltrimethyl Ammonium Bromide Stabilized $Zn_{1+x}SnO_{3+x}$ ($0 \leq x \leq 1$) Nano-Crystallites

Astrid Placke[1,2], Ashok Kumar[1]*, Shashank Priya[3]

1 Department of Physics, National Institute of Technology Kurukshetra, Haryana, 136119, India, **2** Department of Physical Technologies, University of Applied Sciences and Art, Göttingen, 37083, Germany, **3** Center for Energy Harvesting Materials and Systems (CEHMS), Virginia Tech, Blacksburg, Virginia, 24061, United States of America

* ashokku@nitkkr.ac.in

Citation: Placke A, Kumar A, Priya S (2016) Synthesis and Behavior of Cetyltrimethyl Ammonium Bromide Stabilized $Zn_{1+x}SnO_{3+x}$ ($0 \leq x \leq 1$) Nano-Crystallites. PLoS ONE 11(5): e0156246. doi:10.1371/journal.pone.0156246

Editor: Yogendra Kumar Mishra, Institute for Materials Science, GERMANY

Received: October 25, 2015

Accepted: May 11, 2016

Published: May 26, 2016

Data Availability Statement: All relevant data are within the paper and its Supporting Information files. Additional data are available upon request from the corresponding author.

Funding: This work was supported by SERB-DST, Government of India (SERB/F/1769/2013-2014), and a DAAD fellowship to AP.

Competing Interests: The authors have declared that no competing interests exist.

Abstract

We report synthesis of cetyltrimethyl ammonium bromide (CTAB) stabilized $Zn_{1+x}SnO_{3+x}$ ($0 \leq x \leq 1$) nano-crystallites by facile cost-effective wet chemistry route. The X-ray diffraction patterns of as-synthesized powders at the Zn/Sn ratio of 1 exhibited formation of $ZnSn(OH)_6$. Increasing the Zn/Sn ratio further resulted in the precipitation of an additional phase corresponding to $Zn(OH)_2$. The decomposition of these powders at 650°C for 3h led to the formation of the orthorhombic phase of $ZnSnO_3$ and tetragonal SnO_2-type phase of Zn_2SnO_4 at the Zn/Sn ratio of 1 and 2, respectively, with the formation of their mixed phases at intermediate compositions, i.e., at Zn/Sn ratio of 1.25, 1.50 and 1.75, respectively. The lattice parameters of orthorhombic and tetragonal phases were a ~ 3.6203 Å, b ~ 4.2646 Å and c ~ 12.8291Å (for $ZnSnO_3$) and a = b ~ 5.0136 Å and c ~ 3.3055Å (for Zn_2SnO_4). The transmission electron micrographs revealed the formation of nano-crystallites with aspect ratio ~ 2; the length and thickness being 24, 13 nm (for $ZnSnO_3$) and 47, 22 nm (for Zn_2SnO_4), respectively. The estimated direct bandgap values for the $ZnSnO_3$ and Zn_2SnO_4 were found to be 4.21 eV and 4.12 eV, respectively. The ac conductivity values at room temperature (at 10 kHz) for the $ZnSnO_3$ and Zn_2SnO_4 samples were 8.02×10^{-8} Ω^{-1} cm^{-1} and 6.77×10^{-8} Ω^{-1} cm^{-1}, respectively. The relative permittivity was found to increase with increase in temperature, the room temperature values being 14.24 and 25.22 for the samples $ZnSnO_3$ and Zn_2SnO_4, respectively. Both the samples, i.e., $ZnSnO_3$ and Zn_2SnO_4, exhibited low values of loss tangent up to 300 K, the room temperature values being 0.89 and 0.72, respectively. A dye-sensitized solar cell has been fabricated using the optimized sample of zinc stannate photo-anode, i.e., Zn_2SnO_4. The cyclic voltammetry revealed oxidation and reduction around 0.40 V (current density ~ 11.1 mA/cm^2) and 0.57 V (current density– 11.7 mA/cm^2) for Zn_2SnO_4 photo-anode in presence of light.

Introduction

The synthesis of various single cation oxides, e.g., ZnO, TiO_2, SnO_2, MgO, NiO, Fe_2O_3, Nb_2O_3 has been reported by numerous techniques such as sol-gel, hydrothermal, solvo-thermal, solid state reaction, thermal evaporation, co-precipitation, etc. These materials have been used in several applications viz., Li-ion batteries, dye-sensitized solar cells (DSSCs), gas sensors, and photocatalysts for water splitting and organic pollutant degradation [1–11]. The multi-cation oxides have emerged as a potential alternative, and yet rarely been explored for optical devices such as DSSC [4, 12–13]. The perovskite family, i.e., ABO_3 and A_2BO_4 being of special interest because of being chemically, thermally and mechanically stable wide bandgap semiconductor, which can provide high optical transmittance, reduced photo-bleaching, reduced electron-triiodide back recombination rate, and high open circuit voltage [1, 14–16]. Particularly, interest in the zinc stannate ($ZnSnO_3$ and Zn_2SnO_4) nano-crystallites has been surged recently due to their important optical, electrochemical and photoelectrochemical properties and various technological applications in several devices such as light emitting diodes, solar cells, and biosensors [1, 17–20].

Multi-cation material provides flexibility to engineer its physical and/ or chemical behavior by varying the composition [21]. The n-type bi-cation transparent conducting oxide such as ZnO-In_2O_3 has revealed change in its work function, bandgap energy, resistivity and acid etching rate as the function of Zn/In content [22]. The abundance and tunable behavior make these multi-cation compounds interesting for continued research. The $ZnSnO_3$, Zn_2SnO_4 are wide bandgap n-type ternary semiconductor oxides with better corrosion resistance, faster charge injection and faster electron diffusion efficiency than anatase- TiO_2 used in conventional dye-sensitized solar cell. The $ZnSnO_3$, Zn_2SnO_4 and/or intermediate mixed nano-crystalline phases are formed depending upon the Zn/Sn molar ratio of precursor compounds [1]. In general $ZnSnO_3$ precipitates in orthorhombic phase, while Zn_2SnO_4 precipitates in cubic- spinel –type phase [14, 23]. In $ZnSnO_3$, Zn^{2+} and Sn^{4+} cations are distributed at tetrahedral and octahedral sites, respectively, while in Zn_2SnO_4, Zn^{2+} are distributed equally at tetrahedral and octahedral sites, respectively, while Sn^{4+} cations occupy the octahedral sites.

Limited number of studies are available in literature on utilizing Al_2O_3, NiO, ZnO and graphene/ TiO_2 for sensitization of perovskite solar cell [24]. The ternary oxides such as $BaSnO_3$, $ZnSnO_3$ and $Zn_2Sn_2O_4$ have rarely been investigated [4, 24]. In this paper, we report the synthesis of cetyltrimethyl ammonium bromide (CTAB) stabilized $ZnSnO_3$, Zn_2SnO_4 nano-crystallites and their intermediate compositions by facile cost-effective wet chemistry route. These nano-crystallites have been investigated for their structural, optical, dielectric and ac conductivity behavior. Here, an attempt has been made to synthesize tetragonal SnO_2-type phase of Zn_2SnO_4, which has not normally been reported [25]. Many reports have revealed synthesis of $ZnSnO_3$, Zn_2SnO_4 nanostructures of various shapes, e.g., sphere, cube, anisotropic rods, etc. by the use of mineralizers and additives [16]. In present investigation, the particle size and nano-crystallite- type morphology has been realized using surfactant CTAB, which is vital for high absorption of dye and faster electron transport. The facile wet chemistry route utilized for the synthesis has advantage of precisely controlling thermodynamics and kinetic of nucleation and growth of nano-crystallites, which is otherwise difficult to control with other synthesis routes [16, 26].

Materials and Methods

The $ZnSnO_3$, $Zn_{1.25}SnO_{3+\alpha}$, $Zn_{1.5}SnO_{3+\beta}$, $Zn_{1.75}SnO_{3+\gamma}$, Zn_2SnO_4 (where $\alpha \sim 0.25$, $\beta \sim 0.5$, $\gamma \sim 0.75$) nano-crystallites with general formula $Zn_{1+x}SnO_{3+x}$ ($0 \leq x \leq 1$) have been synthesized by facile cost-effective wet chemistry route using cetyltrimethyl ammonium bromide (CTAB)

as a surfactant. First, the aqueous solution of tin chloride pentahydrate ($SnCl_4.5H_2O$) and zinc nitrate hexahydrate ($Zn(NO_3)_2.6H_2O$) in Zn/Sn molar ratio of 1, 1.25, 1.5, 1.75 and 2, respectively in 5 mM individual concentration were prepared through the consistent stirring for 30 min each in separate beakers. Subsequently, $SnCl_4.5H_2O$ and $Zn(NO_3)_2.6H_2O$ solutions in desired amounts were mixed together to obtain another clear solution. Afterward, 5 mM solution of CTAB in the metal (Zn^{2+} and Sn^{2+}) to CTAB molar ratio of 10:1, was added to the above solution drop-wise. These obtained five solutions were dried in oven at 100°C for 12 h, washed with ethanol afterward and subsequently dried for 6 h at 100°C, washed with ethanol again, and dried once more at 100°C for 6h. Now, these dried powders were decomposed at 650°C for 3h to obtain $ZnSnO_3$, $Zn_{1.25}SnO_{3+\alpha}$, $Zn_{1.25}SnO_{3+\beta}$, $Zn_{1.25}SnO_{3+\gamma}$, Zn_2SnO_4 (where $\alpha \sim 0.25$, $\beta \sim 0.5$, $\gamma \sim 0.75$) nano-crystallitess. These obtained five samples were coded as S1, S2, S3, S4 and S5, respectively for further investigation. Fig 1 shows the schematic of the synthesis process.

The phase(s) of the as-synthesized precursor powders and $ZnSnO_3$, $Zn_{1.25}SnO_{3+\alpha}$, $Zn_{1.5}SnO_{3+\beta}$, $Zn_{1.75}SnO_{3+\gamma}$, Zn_2SnO_4 (where $\alpha \sim 0.25$, $\beta \sim 0.5$, $\gamma \sim 0.75$) nano-crystallites with general formula $Zn_{1+x}SnO_{3+x}$ ($0 \leq x \leq 1$) were analyzed by Rigaku Miniflex X-ray diffractometer using Cu $K_{\alpha 1}$ radiation of 1.54056 Å at 30 kV and 15 mA. Morphological characterization of samples S1 and S5 was performed by using transmission electron microscopy Hitachi (model H-7500, 120 kV) equipped with CCD Camera. Diffuse reflectance spectra of powders were recorded by UV-Visible spectrometer; PG instruments Pvt. Ltd. T90+ in the spectral range of 300–1100 nm. Photoluminescence spectra were collected in the wavelength range of 330–450 nm with the excitation wavelength of 290 nm using Simadzu RF-530 spectroflurometer. The impedance analysis at different temperatures was performed using potentiogalvanostat, Biologic SP 240, in the frequency range between 100 Hz to 3MHz. For impedance investigation, the nano-crystalline samples were pelletized in 10 mm diameter pellets at a

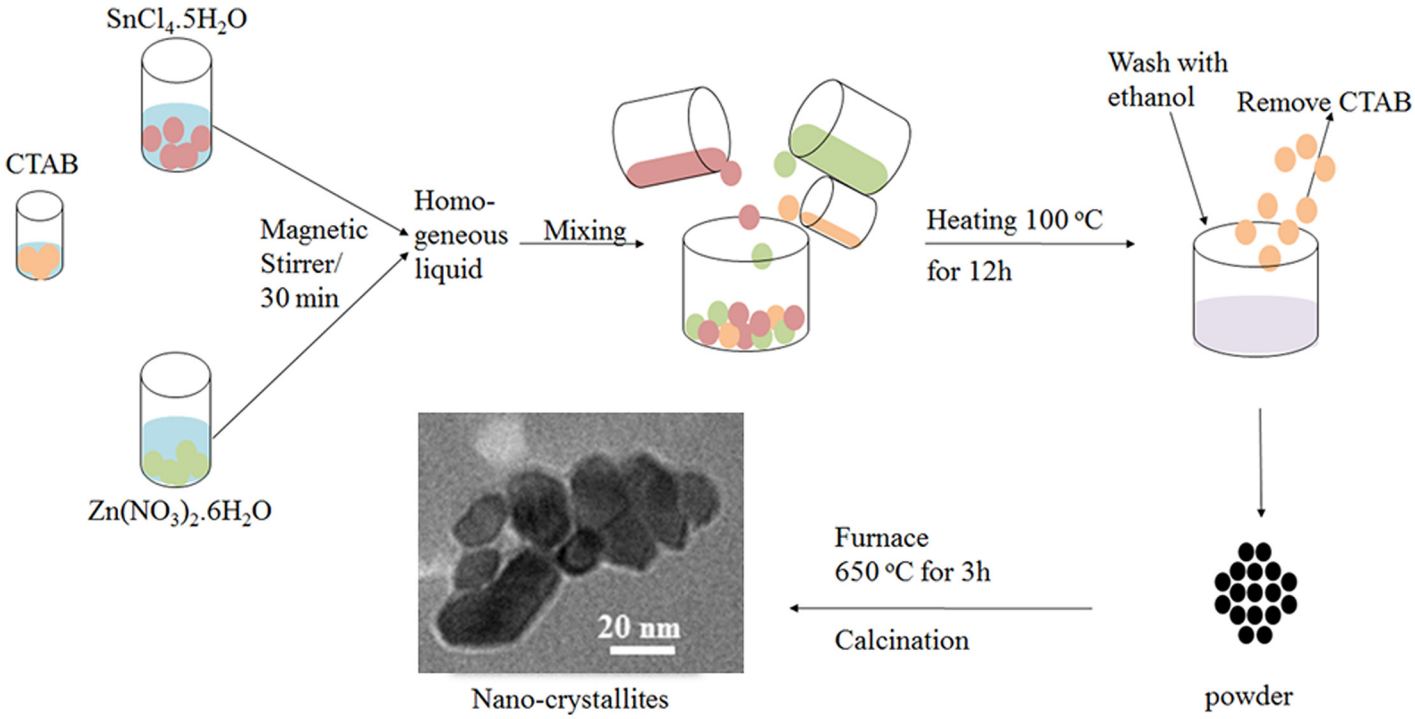

Fig 1. Schematic of the synthesis process.

doi:10.1371/journal.pone.0156246.g001

pressure of 5 ton, sintered at 900°C for 6h, polished subsequently to 1.4 mm thickness, and silver pasted afterward. The dye-sensitized solar cell (DSSC) devices were fabricated using zinc stannate photo-anode, and cyclic voltammetry studies were performed using potentiogalvanostat, Biologic SP 240.

Results and Discussion

3.1 Structural and morphological characterization

Fig 2 shows the X-ray diffraction (XRD) patterns of as-synthesized samples at the Zn/Sn molar ratios of 1 and 2, respectively. The formation of single phase of $ZnSn(OH)_6$ (JCPDS # 20–1455) is evident at Zn/Sn molar ratio of 1. At higher Zn/Sn content, $Zn(OH)_2$ (JCPDS # 72–2032) together with $ZnSn(OH)_6$ phase starts precipitating. Particularly, at the Zn/Sn molar ratio 2, small traces of Zn_2SnO_4 cubic phase (JCPDS # 04–736) together with $ZnSn(OH)_6$ and $Zn(OH)_2$ phases are also observed. The $Zn(OH)_2$ crystallites are presumably oriented in [11] preferred direction as Bragg's reflection planes other than (011) are hardly visible. The observed traces of Zn_2SnO_4 cubic phase too are not visible in the XRD pattern of final compound (Fig 3, discussed later). The mechanism of the reaction can be understood as follows. The $SnCl_4.5H_2O$ and $Zn(NO_3)_2.6H_2O$ in aqueous solution remain dissociated as: $SnCl_4.5H_2O \rightarrow Sn^{4+} + 4Cl^- + 5H_2O$ and $Zn(NO_3)_2.6H_2O \rightarrow Zn^{2+} + 2NO_3^- + 6H_2O$, respectively. The Zn^{2+} and Sn^{4+} ions in Zn/Sn molar ratio of one form a hydroxide as per following reaction: $Zn^{2+} + Sn^{4+} + 6OH^- \rightarrow ZnSn(OH)_6$ [17]. On decomposition at elevated temperature, i.e., 650°C, the $ZnSn(OH)_6$, forms $ZnSnO_3$ as per the reaction $ZnSn(OH)_6 \rightarrow ZnSnO_3 + 3H_2O$. The higher molar ratios of Zn/Sn, i.e., 1.25, 1.5, 1.75 and 2 lead to the precipitation of $Zn(OH)_4^{2-}$ together with the precipitation of $ZnSn(OH)_6$ as per the following additional reaction, $Zn^{2+} + 2OH^- \rightarrow Zn(OH)_4^{2-}$. The $Zn(OH)_4^{2-}$ reacts with $ZnSn(OH)_6$ and forms Zn_2SnO_4 as per the reaction, $ZnSn(OH)_6 + Zn(OH)_4^{2-} \rightarrow Zn_2SnO_4 + 4H_2O + 2OH^-$. It is obvious that when molar ratio of Zn/Sn is fractional number between 1 and 2, the precipitation of both $ZnSnO_3$ and Zn_2SnO_4 phases will occur. The presence of the surfactant possibly alters the surface energy of the crystallites surfaces and, in turn, results in the anisotropic growth of nanoparticles. In the present work, the CTAB, which has been used as a surfactant, plays a pivotal role in monodispersion of the as synthesized nanocrystallites [27].

Fig 3 shows the X-ray diffraction patterns of the $ZnSnO_3$, $Zn_{1.25}SnO_{3+\alpha}$, $Zn_{1.5}SnO_{3+\beta}$, $Zn_{1.75}SnO_{3+\gamma}$, Zn_2SnO_4 (where $\alpha \sim 0.25$, $\beta \sim 0.5$, $\gamma \sim 0.75$) nano-crystallites obtained by decomposition of the gel product (formed through wet chemistry reaction at 100°C for 18 h) at 650°C for 3h. At Zn/Sn molar ratio of 1, it clearly indicates the formation of orthorhombic type-$ZnSnO_3$ (JCPDS # 28–1486) with the values of lattice parameters being as a ~ 3.6203 Å, b ~ 4.2646 Å and c ~ 12.8291Å. On increasing the Zn/Sn molar ratio to 2, the structure revealed formation of single phase of tetragonal SnO_2 –type Zn_2SnO_4 (JCPDS # 88–0287), with mixed phases of $ZnSnO_3$ and Zn_2SnO_4 at intermediate compositions (i.e., at Zn/Sn molar ratio of 1.25, 1.50, 1.75). The crystallite sizes were estimated using the Bragg relation, i.e., $D = 0.9\lambda/\beta\cos\theta$, where D is average crystallite size, λ wavelength of the X-ray used, β, corrected full width at half maximum (FWHM) of the respective peak belonging to diffraction angle 2θ. The estimated values of crystallite size for samples S1, S2, S3, S4 and S5 were found to be 47, 58, 48, 51, and 49 nm, respectively. At Zn/Sn molar ratio of 1, the average crystallite size was 47 nm, which increased to 58 nm at Zn/Sn molar ratio of 1.25. The coordination numbers of Zn^{2+} and Sn^{4+} ions in orthorhombic $ZnSnO_3$ are 4 and 6, respectively. Further, the ionic radii of Sn^{4+} and Zn^{2+} ions in six-coordination are 0.69 Å, and 0.74 Å, respectively. Obviously, the ionic radius of $Zn^{2+}$is higher than Sn^{4+}, therefore on occupying Sn^{4+} lattice sites in the $ZnSnO_3$ crystal, it will put crystal under tensile stress, which, in turn, will give rise to increase crystallite size

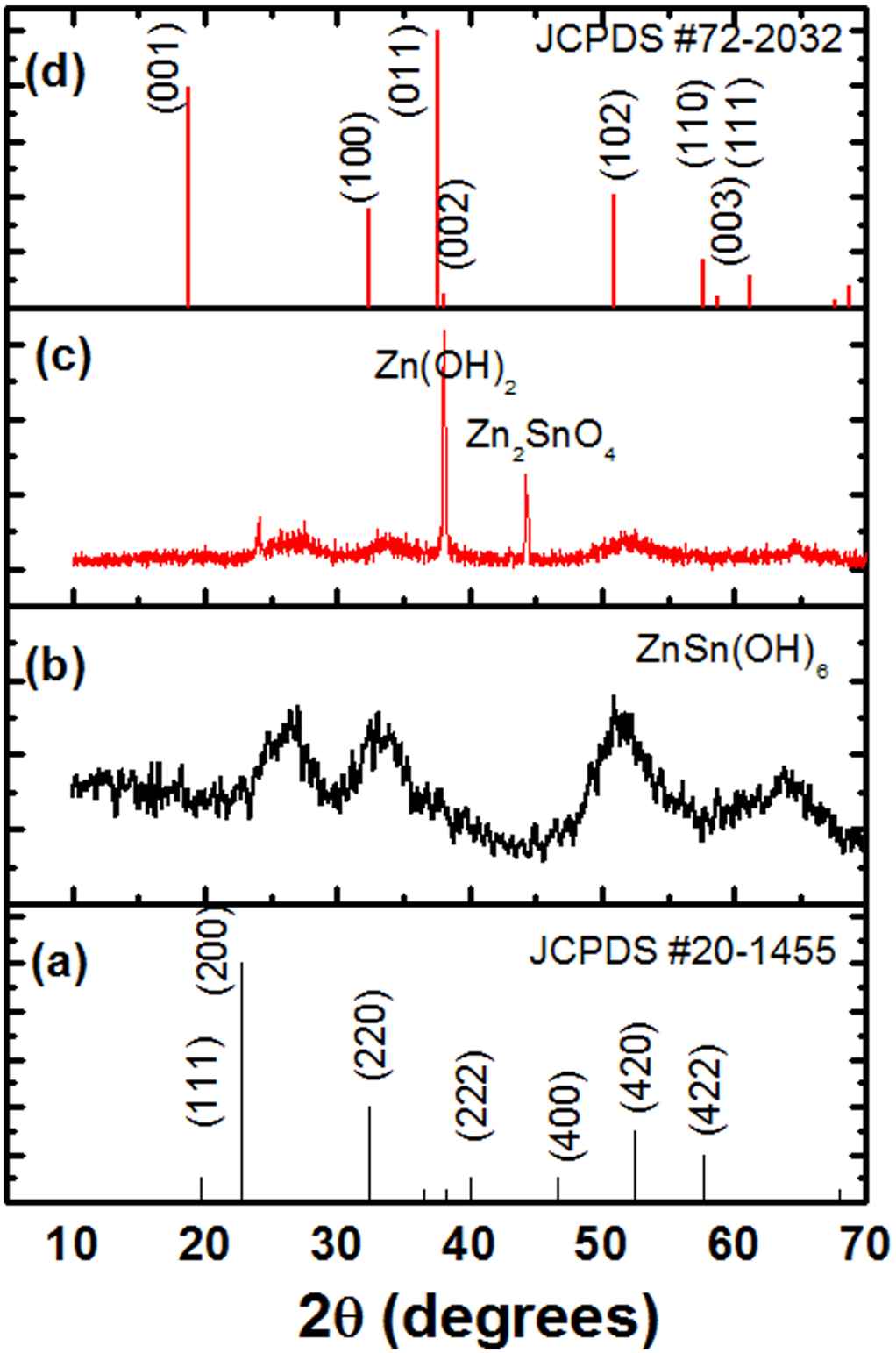

Fig 2. X-ray diffraction patterns of standard JCPDS cards 20–1455 and 72–2052 (a, c) and as-synthesized samples at the Zn/Sn molar ratios of 1 and 2 (b, d).

doi:10.1371/journal.pone.0156246.g002

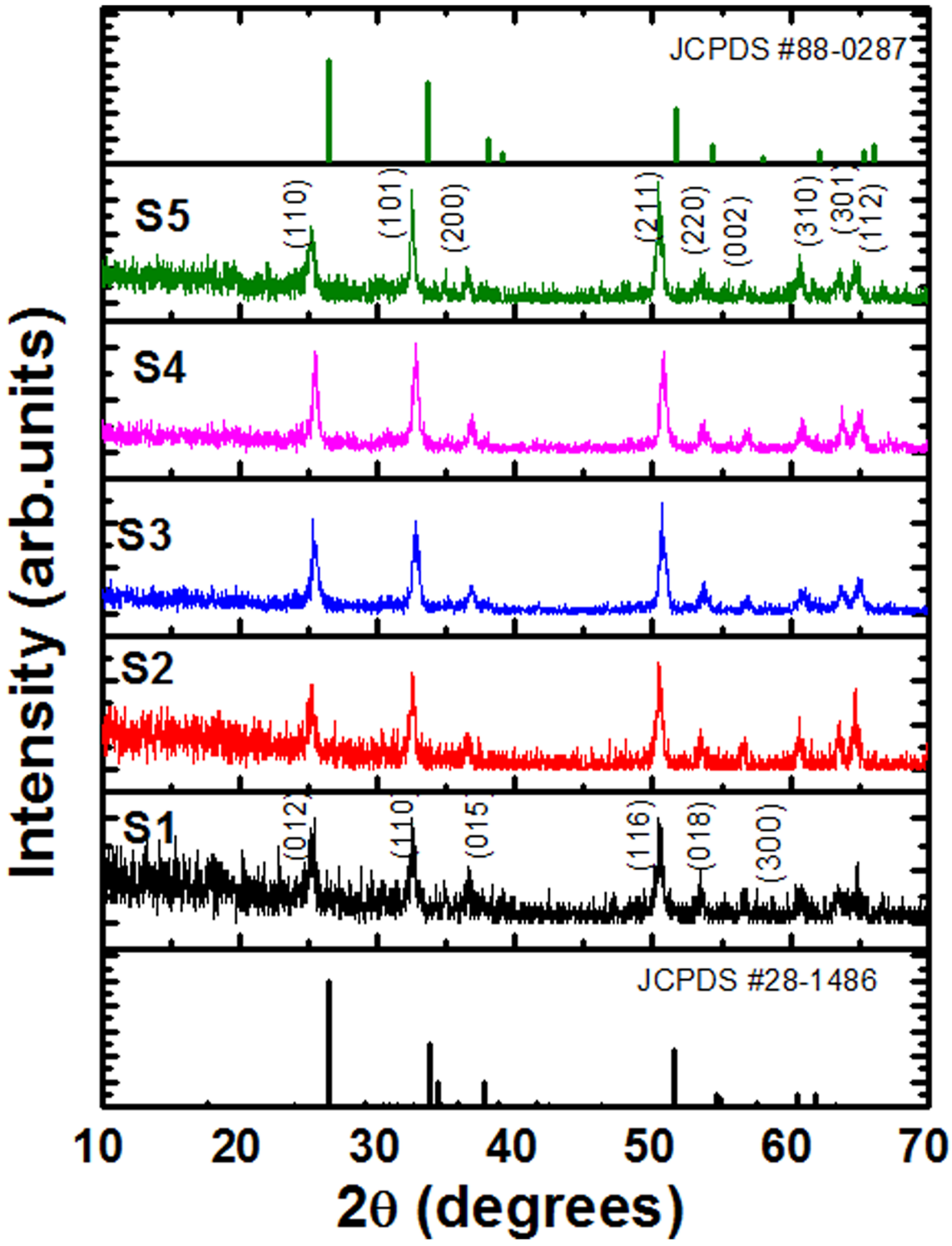

Fig 3. X-ray diffraction patterns of samples S1, S2, S3, S4, and S5 i.e., of the $ZnSnO_3$, $Zn_{1.25}SnO_{3+\alpha}$, $Zn_{1.5}SnO_{3+\beta}$, $Zn_{1.75}SnO_{3+\gamma}$, Zn_2SnO_4 nano-crystallites, respectively obtained by decomposition of the gel product (formed through wet chemistry reaction at 100°C for 18 h) at 650°C for 3h.

doi:10.1371/journal.pone.0156246.g003

[28–29]. On increasing the Zn/Sn molar ratio to 1.5, the precipitation of secondary phase, i.e., Zn_2SnO_4 becomes significant to inhibit the growth of primary phase crystallites, i.e., $ZnSnO_3$. Due to this reason the crystallite size of sample S3 has been found to be smaller than the sample S2. At Zn/Sn molar ratio of 1.75, i.e., for sample S4, the size increased slightly in comparison to sample S3, which may be due to the fact that sample S4 at Zn/Sn molar ratio of 1.75 will have higher amount of tetragonal Zn_2SnO_4 phase formation than sample S3. In contrary to sample S2, where primary phase was orthorhombic type- $ZnSnO_3$, in this case, the primary phase is Zn_2SnO_4. As discussed before, in case of sample S2, the lower amount of Zn_2SnO_4 phase was not able to inhibit the growth of $ZnSnO_3$. Similarly in present case the lower amount of $ZnSnO_3$ phase is not able to inhibit the growth of Zn_2SnO_4 crystallites, and, in turn, exhibit increased crystallite size than sample S3. Further increase in Zn/Sn molar ratio (Zn/Sn = 2) reveals a slight decrease in crystallite size (~ 49 nm), possibly due to inherent oxygen vacancies in Zn_2SnO_4, which, put crystal under compressive stress. The values of lattice parameters for tetragonal Zn_2SnO_4 were as a = b ~ 5.0136 Å and c ~3.3055Å.

Fig 4 shows transmission electron micrographs of $ZnSnO_3$ and Zn_2SnO_4 samples, i.e., for samples S1 and S5. The sample S1 exhibits nano-rod type morphology with average aspect ratio of ~2; the length and thickness being as ~24 nm and ~13 nm, respectively. The sample S5 retains the similar morphology; the average crystallite length being ~ 47 nm and thickness ~22 nm, respectively. The average aspect ratio remains almost same. It is obvious that crystallite size obtained via transmission electron microscopy (TEM) observations are smaller than that of estimated from X-ray diffraction line broadening using Scherrer equation. The possible reason may be settling down of large particles during TEM sample preparation.

3.2 Optical characterization

S1 Fig shows diffused reflectance spectra of the samples S1, S2, S3, S4 and S5, i.e., $ZnSnO_3$, $Zn_{1.25}SnO_{3+\alpha}$, $Zn_{1.5}SnO_{3+\beta}$, $Zn_{1.75}SnO_{3+\gamma}$, Zn_2SnO_4 (where $\alpha \sim 0.25$, $\beta \sim 0.5$, $\gamma \sim 0.75$) nano-crystallites obtained by decomposition of the gel product (formed through wet chemistry reaction at 100°C for 18 h) at 650°C for 3h. As per optical absorbance and Kubelka-Munk function, the pure diffuse reflectance of the sample can be expressed as [30],

$$F(R_{pd}) = (1 - R_{pd})^2 / 2R_{pd} = K/S \quad (1)$$

where R_{pd} is the pure diffuse reflectance, K is absorption coefficient and S is scattering coefficient. The pure diffuse reflectance, $F(R_{pd})$ is proportional to the molar absorption coefficient (α). The relation between optical bandgap (E_g) and α can be given by well-known Tauc relation [30],

$$(\alpha h\upsilon) = C(h\upsilon - E_g)^n \quad (2)$$

where $h\upsilon$ is the energy of the absorbed photon, and C is proportionality constant. Also, from Eqs 1 and 2, following relations can be obtained [31–33],

$$[(F(R_{pd})h\upsilon] = C(h\upsilon - E_g)^n \quad (3)$$

where n equals to ½ for allowed direct transition, 1 for non-metallic materials, 3/2 for direct forbidden transitions, 2 for allowed indirect transitions and 3 for indirect forbidden transitions, respectively [31–33]. For estimation of bandgap values, the $[(F(R_{pd})h\upsilon]^{1/n}$ versus $h\upsilon$ plots are extrapolated to linear fitted region at $[(F(R_{pd})h\upsilon]^{1/n} = 0$.

The $ZnSnO_3$ and Zn_2SnO_4 are known to be direct wide bandgap semiconductors [34–38]. Therefore, direct bandgap values have been estimated using Eq 3, absorption data of S1 Fig and

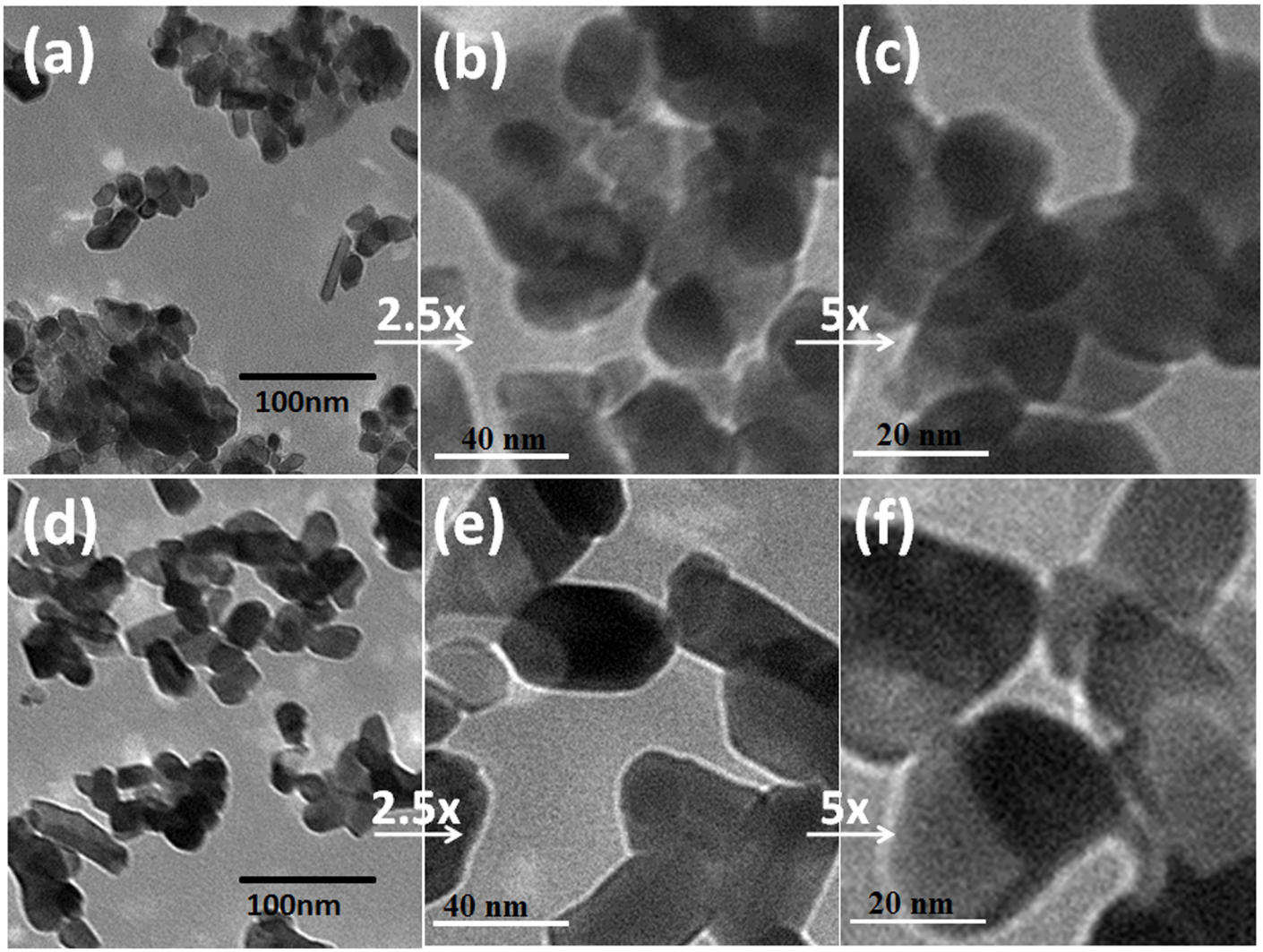

Fig 4. (a-c) transmission electron micrographs of $ZnSnO_3$ (S1) and (d-f) of Zn_2SnO_4 (S5) samples.

doi:10.1371/journal.pone.0156246.g004

are shown in Fig 5. The estimated values of bandgap are 4.21, 3.62, 3.00, 3.77 and 4.12 eV for samples S1, S2, S3, S4 and S5, i.e., $ZnSnO_3$, $Zn_{1.25}SnO_{3+\alpha}$, $Zn_{1.5}SnO_{3+\beta}$, $Zn_{1.75}SnO_{3+\gamma}$, Zn_2SnO_4 (where $\alpha \sim 0.25$, $\beta \sim 0.5$, $\gamma \sim 0.75$) nano-crystallites, respectively. The reported values of band-gap for $ZnSnO_3$ and Zn_2SnO_4 bulk samples are 3.4–3.9 eV [39–41] and 3.3 eV [41], respectively. Not many reports are available on the bandgap studies of $ZnSnO_3$, and further the absorbance data of Zn_2SnO_4 have been debated [34–38]. Therefore, these samples have further been investigated using photoluminescence studies.

Fig 6 show the emission spectra of the samples S1, S2, S3, S4 and S5, i.e., $ZnSnO_3$, $Zn_{1.25}SnO_{3+\alpha}$, $Zn_{1.5}SnO_{3+\beta}$, $Zn_{1.75}SnO_{3+\gamma}$, Zn_2SnO_4 obtained at the excitation wavelength of 290 nm. It is evident that in case of sample S1, i.e. $ZnSnO_3$, the emission peak occurs at the wavelength of around 365 nm (energy ~ 3.40 eV). The increase in Zn/Sn molar ratio to 1.25, leads to slight redshift in peak energy ~ 3.39 eV, and at Zn/Sn molar ratio of 1.5 to 3.38 eV. Afterward, it retains its position till Zn/Sn molar ratio to 1.75. At Zn/Sn molar ratio of 2, the peak exhibits a little blue-shift in energy ~ 3.39 eV.

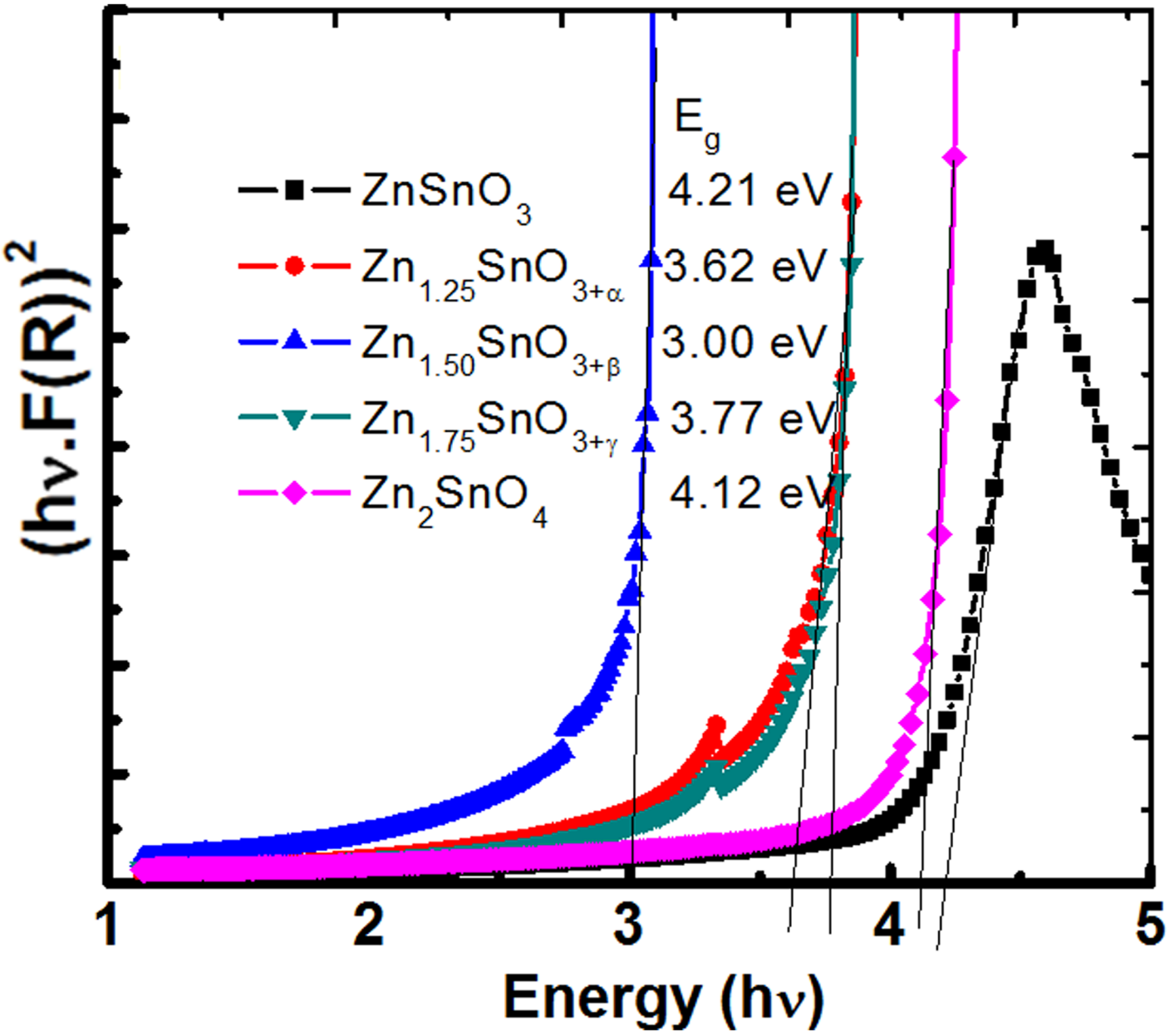

Fig 5. Band gap estimation of $ZnSnO_3$, $Zn_{1.25}SnO_{3+\alpha}$, $Zn_{1.5}SnO_{3+\beta}$, $Zn_{1.75}SnO_{3+\gamma}$, Zn_2SnO_4 nano-crystallites from diffused reflectance spectra (S1 Fig) obtained by decomposition of the gel product at 650°C for 3h.

doi:10.1371/journal.pone.0156246.g005

In fact samples S2, S3 and S4 are dual phase composites of the nano-crystalline $ZnSnO_3$, and Zn_2SnO_4 semiconductors. Assuming that at Zn/Sn ratio of 1, 1.25, 1.5, 1.75 and 2, the precipitated phases are of pure $ZnSnO_3$, and Zn_2SnO_4 nano-crystalline semiconductors only, the ratios of $ZnSnO_3$ to Zn_2SnO_4 phases at Zn/Sn molar ratios of 1, 1.25, 1.5, 1.75 and 2, should be 1::0, 0.75::0.25, 0.5::0.5, 0.25::0.75, and 0::1, respectively. Following the simple mixture rule the estimated bandgap values should be as 4.21, 4.19, 4.17, 4.14 and 4.12 eV, respectively (as the estimated bandgap values for semiconductors $ZnSnO_3$, and Zn_2SnO_4 are 4.21 and 4.12 eV, respectively). The deviation in estimated bandgap values is substantial for intermediate composite samples, i.e., samples S2, S3 and S4. Further, the emission spectra do not show such

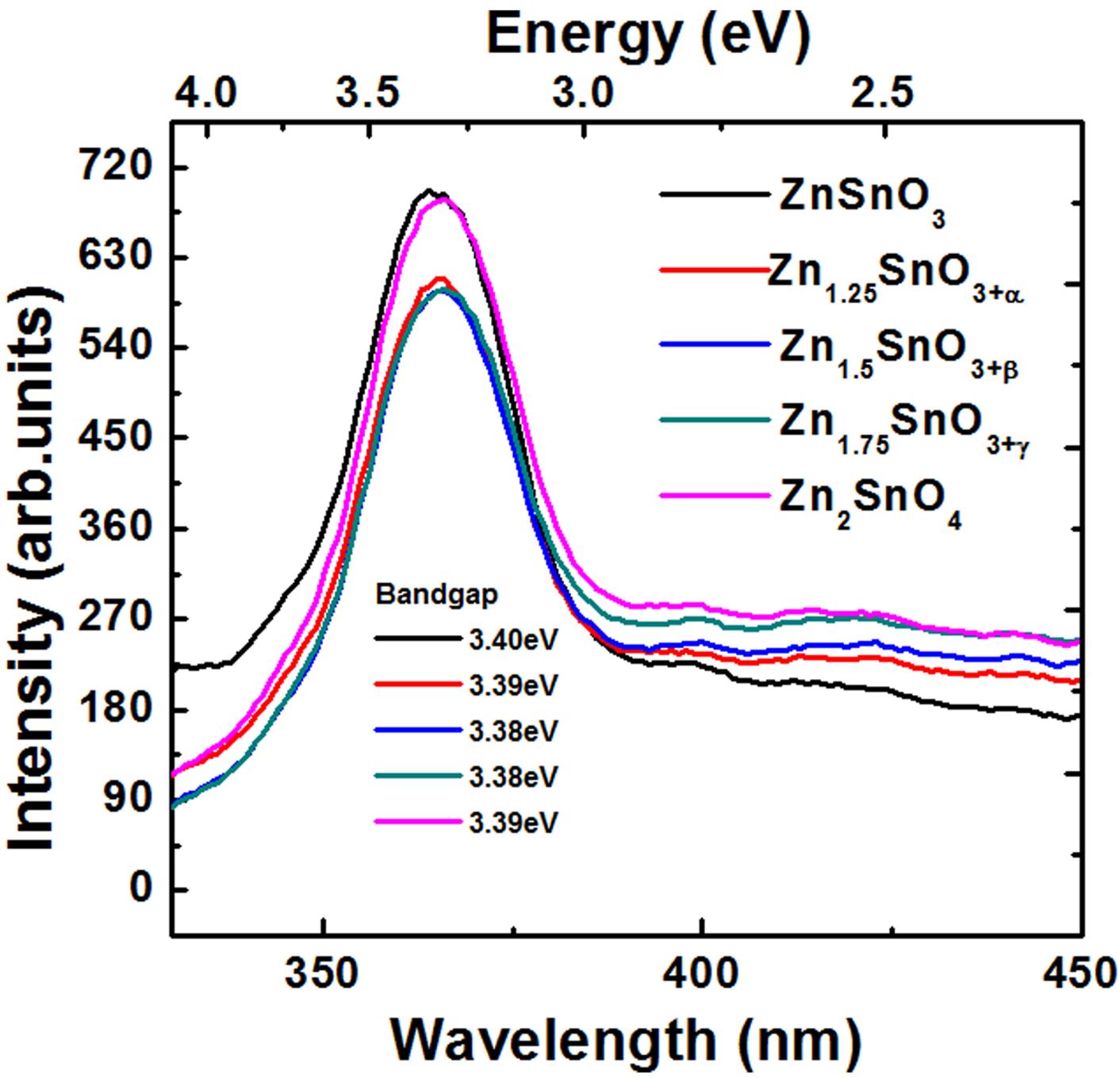

Fig 6. Emission spectra of $ZnSnO_3$, $Zn_{1.25}SnO_{3+\alpha}$, $Zn_{1.5}SnO_{3+\beta}$, $Zn_{1.75}SnO_{3+\gamma}$, Zn_2SnO_4 obtained at the excitation wavelength of 290 nm.

doi:10.1371/journal.pone.0156246.g006

drastic variation in bandgap. It indicates that somehow the diffused reflectance curves of intermediate samples which results due to overlapping of two phase compounds propagate more errors in bandgap estimation, i.e., the assumption of considering the intermediate samples as single phase and estimation of the bandgap does not fits well. As discussed before, the fact of dual phase formation in intermediate compounds has been verified through XRD investigation and is shown in Fig 3. To understand the these samples further, the excitation spectra of

samples S1 and S5 were collected at the emission wavelength of 366 nm and are shown in S2 Fig. These show excitation at almost same wavelength as emission; indicating direct bandgap semiconductor nature of these samples. It is obvious that photoluminescence investigation (emission and absorption spectra) is more close to experimentally reported bandgap values [39–41] in comparison to estimated bandgap values using diffused reflectance spectra.

3.3 Variation of ac conductivity, permittivity and loss tangent

Fig 7(a) and 7(b) shows variation of ac conductivity with frequency in the temperature range up to 473 K. The conductivity variation as a function of temperature can be shown as $\sigma(\omega) = \omega\varepsilon_o\varepsilon'\tan(\delta)$ [42], where ε_o, ε', and $\tan(\delta)$ are permittivity of free space, relative permittivity of the sample, and loss tangent, respectively at the frequency ω. Obviously, the conductivity increases with frequency as well as with temperature (Fig 7a and 7b) for both the samples $ZnSnO_3$ and Zn_2SnO_4. The ac conductivity values for the sample $ZnSnO_3$ at the frequency of 10 kHz are $8.02\times10^{-8}\Omega^{-1}$ cm^{-1}, $8.72\times10^{-8}\Omega^{-1}$ cm^{-1} and $7.68\times10^{-7}\Omega^{-1}$ cm^{-1} for the temperature of 300, 373 and 473 K, respectively. It is evident that the conductivity values increase with the increase in temperature as more charge carriers become available for conduction at increased

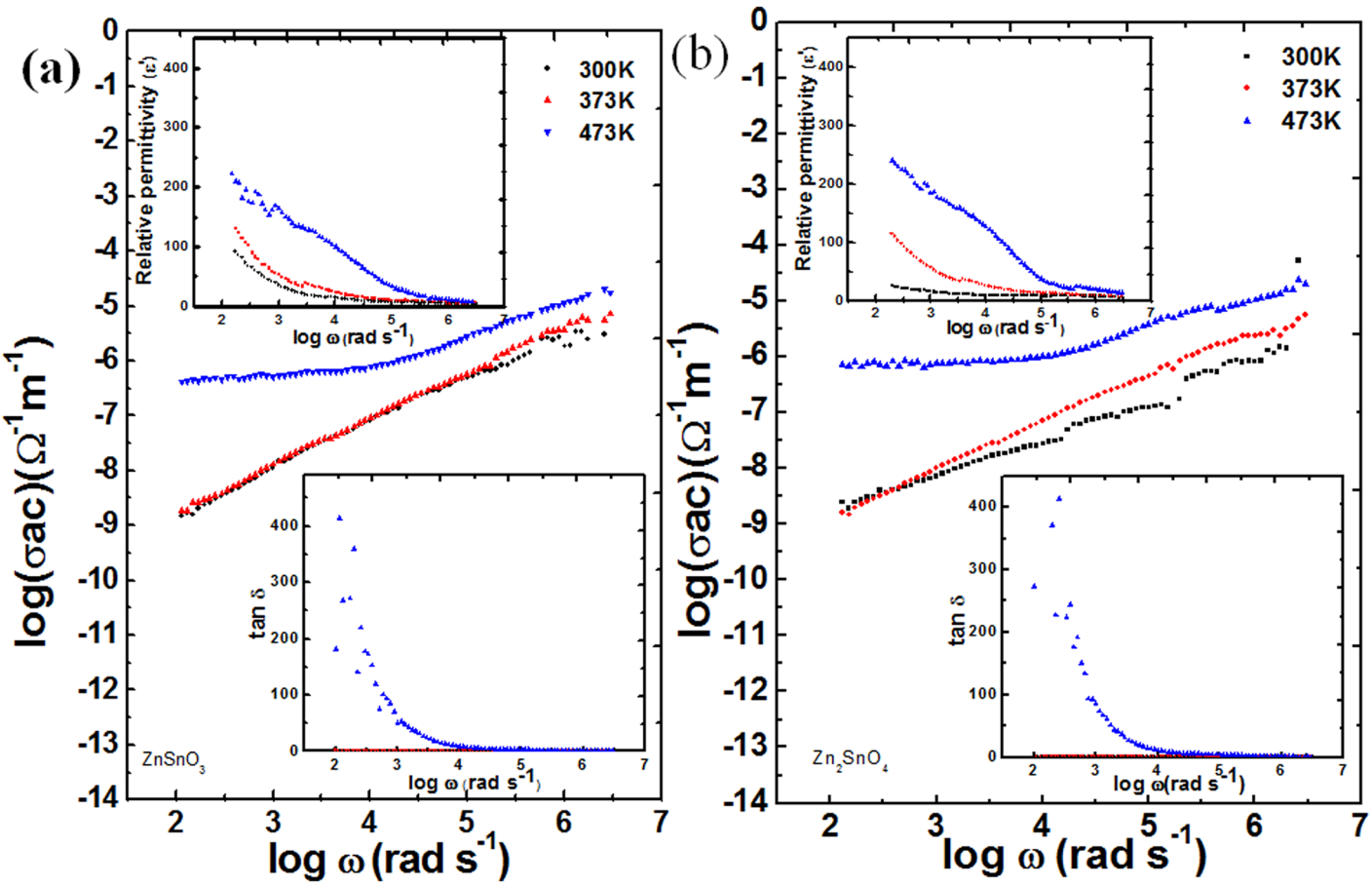

Fig 7. (a, b) variation of ac conductivity with frequency at temperature range up to 473 K, top left corner inset shows variation of relative permittivity with frequency for samples $ZnSnO_3$ (Fig 7a) and Zn_2SnO_4 (Fig 7b), bottom right corner insets show loss tangent as the function of frequency for $ZnSnO_3$ and Zn_2SnO_4, respectively.

doi:10.1371/journal.pone.0156246.g007

temperature. The ac conductivity values for Zn_2SnO_4 nano-crystalline sample at the frequency of 10 kHz were found to be 6.77×10^{-8} Ω^{-1} cm^{-1}, 8.06×10^{-8} Ω^{-1} cm^{-1} and 1.00×10^{-6} Ω^{-1} cm^{-1}. Clearly, the conductivity values for the sample Zn_2SnO_4 are lower than $ZnSnO_3$ upto the temperature of 373 K, and subsequently become higher at the temperature of 473 K. This may be ascribed to its different crystal structure (crystal structure of Zn_2SnO_4 and $ZnSnO_3$ are tetragonal and orthorhombic, respectively), which leads to different crystal defects. The number of oxygen defects is possibly higher in $Zn_2SnO_{4-\Delta}$, (where Δ shows oxygen defects) in comparison to $ZnSnO_{3-\blacktriangle}$ (where ▲ shows oxygen defects) samples, which, in turn lead to higher charge carrier density at elevated temperatures. This fact has also been discussed in structural analysis Section 3.1 for the explanation of reduced crystallite size at the Zn/Sn ratio of 2.

Top left corner insets of Fig 7(a) and 7(b) show variation of relative permittivity with frequency for samples $ZnSnO_3$ and Zn_2SnO_4, respectively. Both of these samples exhibit a plateau region; and clear dispersive nature at lower frequencies. Particularly, at 10 kHz the values of relative permittivity for sample $ZnSnO_3$ are 14.24, 20.83 and 103.90 at the temperature of 300, 373 and 473 K, respectively. The values of relative permittivity for Zn_2SnO_4 sample are higher than $ZnSnO_3$ samples at the same temperature values, and have been observed as 25.33, 34.00, and 124.61, respectively. The relative permittivity decreases with increase in frequency due to deformation and relaxation polarization. The deformation and relaxation depend on displacement and orientation of charge carriers, respectively. Moreover, at higher frequencies molecular dipoles take more time to reorient and thereby lead to decrease in orientation polarization. The relative permittivity values for Zn_2SnO_4 sample are higher than $ZnSnO_3$ samples. Also, as discussed before, optical absorbance studies revealed that the estimated bandgap values for the samples $ZnSnO_3$ and Zn_2SnO_4 as 4.21 and 4.12 eV (direct bandgap), respectively. According to electric polarizability phenomenon the decrease in bandgap leads to increase in the values of the relative permittivity.

Insets of Fig 7(a) and 7(b), at bottom right corner, shows the variation of loss tangent as the function of frequency for the samples $ZnSnO_3$and Zn_2SnO_4, respectively. The loss tangent values for the sample $ZnSnO_3$ are 0.89, 0.92, and 8.81, respectively at the temperature of 300, 373 and 473 K, respectively. The values of loss tangent for the sample Zn_2SnO_4 are 0.72, 0.86 and 10.15, respectively at the temperature of 300, 373 and 473 K, respectively. The values of loss tangent for both the samples at 473 K are increased considerably due to increased phonon energy at elevated temperatures caused by increased thermal vibrations.

3.4 Cyclic voltammetry of dye-sensitized solar cell

Fig 8 shows cyclic voltammogram of the typical DSSC device (in light and no light conditions) of area 4×6 mm^2 fabricated using ITO coated glass, zinc stannate photo-anode (Zn_2SnO_4), platinum counter electrode, I^-/I_3^- electrolyte, and N749 dye. The I^-/I_3^-electrolyte was synthesized by using Imidazolium iodide 0.7 M (0.8824 g) I_2 0.03 M (0.0381g), GSCN (Guanidine thiocyanate), 0.05 M (0.0305 g), TBP (4-tert-butylpyridine), 0.5 M (0.3414 g) and ACN/VN (acetonitrile/valeronitrile) (85:15), 4.25 ml: 0.75 ml. In absence of light, oxidation ($3I^- \rightarrow I_3^- + 2e$) or reduction ($I_3^- + 2e \rightarrow 3I^-$) peaks are not clearly visible, which indicates that there is no sufficient change transfer from platinum electrode. However, in light conditions there is more obvious change transfer. The oxidation and reduction peaks are observed at 0.40 V (current density ~ 11.1 mA/cm^2) and, 0.57 V (current density– 11.7 mA/cm^2), respectively; indicating good performance of the device. The cyclic voltammetry (CV) is a very versatile technique to investigate electron-transfer properties of the electrodes. Lan et. al. [43] used CV to compare the catalytic activity of various counter electrodes used is DSSC.

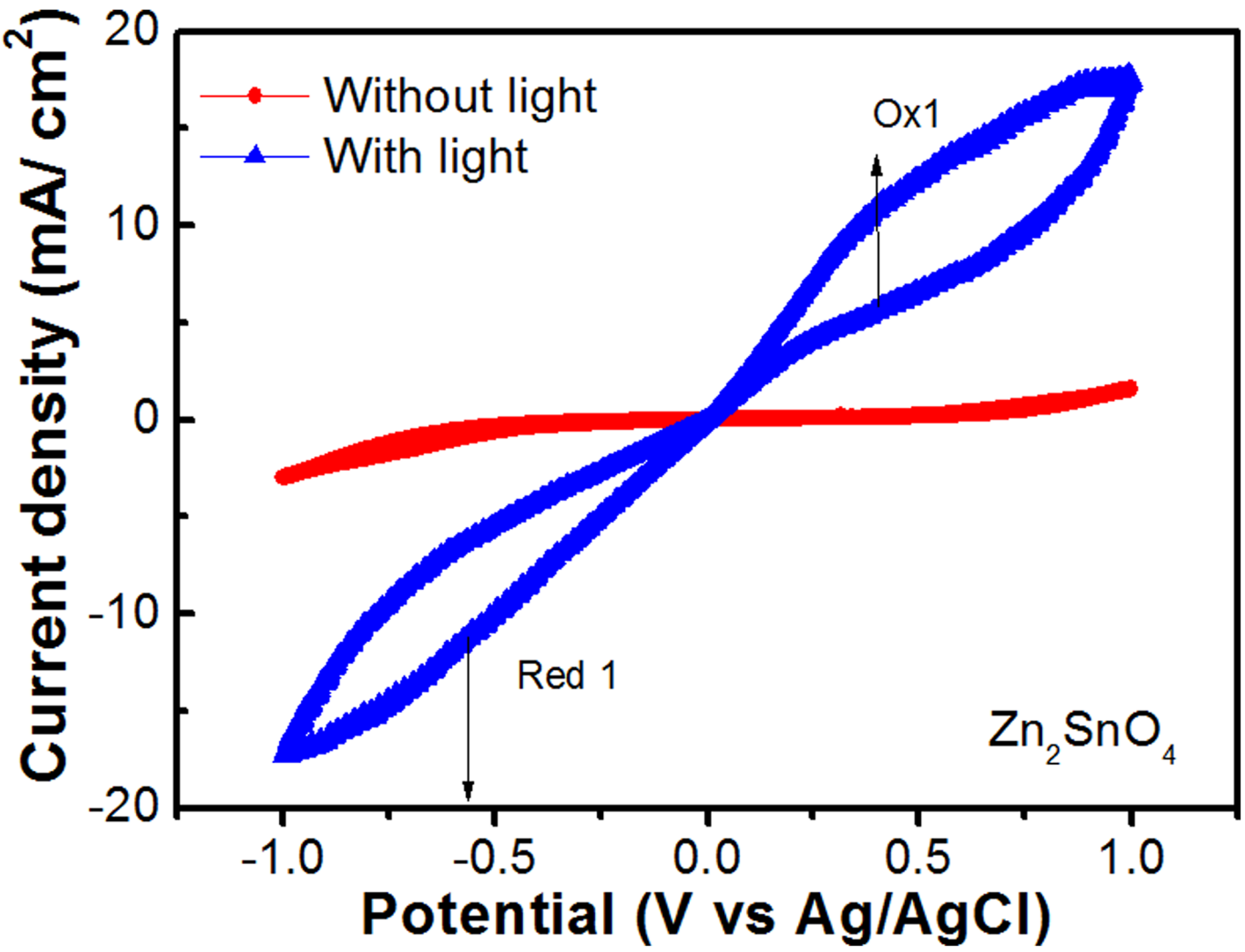

Fig 8. Electron-transfer properties of the electrode using cyclic voltammetry (CV) in $I^-/I3-$ electrolyte composition with Zn_2SnO_4 photo-anode.

doi:10.1371/journal.pone.0156246.g008

Conclusions

The cetyltrimethyl ammonium bromide (CTAB) stabilized $Zn_{1+x}SnO_{3+x}$ ($0 \leq x \leq 1$) nano-crystallites have successfully been synthesized using facile cost-effective wet chemistry route. The structural analysis confirmed the formation of orthorhombic $ZnSnO_3$, tetragonal SnO_2-type Zn_2SnO_4 and/or their mixed phases depending upon the Zn/Sn ratio of the precursors. The morphological analysis exhibited $ZnSnO_3$ crystallites to be approximately of the half size that of Zn_2SnO_4 crystallites (the length and thickness being 24, 13 for $ZnSnO_3$ and 47, 22 nm for Zn_2SnO_4), respectively with aspect ratio of 2. The UV-visible diffuse reflectance together with photoluminescence data revealed these nano-crystallites to be direct wide bandgap semi-conductors. The emission spectra exhibited bandgap of these nano-crystallites to be ~3.40 eV. Further, the room temperature ac conductivity values for the $ZnSnO_3$ were found to be higher than Zn_2SnO_4 samples. The cyclic voltammetry analysis of $ZnSnO_3$ and Zn_2SnO_4 photo-anode based dye-sensitized solar cell revealed oxidation and reduction around 0.40 V and, 0.57V, respectively.

Supporting Information

S1 Fig. Diffused reflectance spectra of $ZnSnO_3$, $Zn_{1.25}SnO_{3+\alpha}$, $Zn_{1.5}SnO_{3+\beta}$, $Zn_{1.75}SnO_{3+\gamma}$, Zn_2SnO_4 nano-crystallites obtained by decomposition of the gel product at 650°C for 3h.
(TIF)

S2 Fig. Excitation spectra of $ZnSnO_3$ and Zn_2SnO_4 nano-crystallites at the emission wavelength of 366 nm.
(TIF)

S1 File. Data of Fig 2.
(XLSX)

S2 File. Data of Fig 3.
(XLSX)

S3 File. Data of Fig 6.
(XLSX)

S4 File. Data of Fig 7.
(XLSX)

S5 File. Data of Fig 8.
(XLSX)

Acknowledgments

One of the authors (A.P.) wishes to thank German Academic Exchange Service (DAAD) for providing her fellowship to carry out this work and Mr. Anil Kumar for help during experimental work. This work was supported by SERB-DST, Government of India (SERB/F/1769/2013-2014).

Author Contributions

Conceived and designed the experiments: AP AK SP. Performed the experiments: AP AK. Analyzed the data: AP AK SP. Contributed reagents/materials/analysis tools: AP AK SP. Wrote the paper: AP AK SP.

References

1. Miyauchi M, Liu Z, Zhao ZG, Anandan S, Hara K. Single crystalline zinc stannate nanoparticles for efficient photo-electrochemical devices. Chem. Commun. 2010; 46: 1529–1531.
2. Jia T, Zhao J, Fu F, Deng Z, Wang W, Fu Z et al. Synthesis, characterization, and photocatalytic activity of Zn-doped SnO_2/Zn_2SnO_4 coupled nanocomposites. Int. J. Photoenerg. 2014; 2014: 197824 (7 pp.).
3. Suhaimi S, Shahimin MM, Alahmed ZA, Chyský J, Reshak AH. Materials for enhanced dye-sensitized solar cell performance: Electrochemical application. Int. J. Electrochem. 2015; 10: 2859–2871.
4. Tan B, Toman E, Li Y, Wu Y. Zinc Stannate (Zn_2SnO_4), dye-sensitized solar cells. J. Am. Chem. Soc. 2007; 129: 4162–4163. PMID: 17371032
5. Zou Z, Ye J, Sayama K, Arakawa H. Direct splitting of water under visible light irradiation with an oxide semiconductor photocatalyst. Nature. 2001; 414: 625–627. PMID: 11740556
6. Paulowicz I, Hrkac V, Kaps S, Cretu V, Lupan O, Braniste T, et al. Three-dimensional SnO_2 nanowire networks for multifunctional applications: From high-temperature stretchable ceramics to ultraresponsive sensors. Adv. Electron. Mater. 2015; 1: 1500081.
7. Zhao Y, Yan Y, Kumar A, Wang H, Porter WD, Priya S. Thermal conductivity of self-assembled nanostructured ZnO bulk ceramics. J. Appl. Phys. 2012; 112: 034313(1–6).

8. Najim M, Modi G, Mishra YK, Adelung R, Singh D, Agarwal V. Ultra-wide bandwidth with enhanced microwave absorption of electroless Ni–P coated tetrapod-shaped ZnO nano- and microstructures, Phys. Chem. Chem. Phys. 2015; 17: 22923–22933. doi: 10.1039/c5cp03488d PMID: 26267361
9. Kumar V, Gohain M, Som S, Kumar V, Bezuindenhoudt BCB, Swart HC. Microwave assisted synthesis of ZnO nanoparticles for lighting and dye removal application. Physica B. 2016; 480: 36–41.
10. Lupan O, Cretu V, Postica V, Ababii N, Polonskyi O, Kaidas V, et al. Enhanced ethanol vapour sensing performances of copper oxide nanocrystals with mixed phases, Sensors Actuator. B. 2016; 224: 434–448.
11. Kumar V, Kumar V, Som S, Neethling JH, Lee M, Ntwaeaborwa OM, et al. The role of surface and deep-level defects on the emission of tin oxide quantum dots. Nanotechnol. 2014; 25: 135701 (9pp).
12. Hwang D, Jin JS, Lee H, Kim HJ, Chung H, Kim DY, et al. Hierarchically structured Zn_2SnO_4 nano-beads for high-efficiency dye-sensitized solar cells. Sci. Rep. 2014; 4: 07353 (7pp.).
13. Minami T. New n-type transparent conducting oxides, MRS Bull. 2000; 25: 38–44.
14. Chen YC, Chang YH, Tsai BS. Photoluminescent properties of europium-activated Zn_2SnO_4 phosphors, Mater. Trans. 2004; 45: 1684–1686.
15. Suzuki Y, Okamoto Y, Ishii N. Dye-sensitized solar cells using double-oxide electrodes: A brief review. J. Phys. Confer. Ser. 2015; 4: 596 (4pp.).
16. Baruah S, Dutta J. Zinc stannate nanostructures: Hydrothermal synthesis. Sci. Technol. Adv. Mater. 2011; 12: 013004 (18pp.).
17. Zhao Y, Hu L, Liu H, Liao M, Fang X, Wu L. Band gap tunable Zn_2SnO_4 nanocubes through thermal effect and their outstanding ultraviolet light photoresponse. Sci. Rep. 2014; 4: 6847 (7pp.). doi: 10.1038/srep06847 PMID: 25355096
18. Singh R, Yadav AK, Gautam C. Synthesis and humidity sensing investigations of nanostructured $ZnSnO_3$. J. Sensor Technol. 2011; 1: 116–124.
19. Yang HG, Sun CH, Qiao SZ, Zou J, Liu G, Smith SC, et al. Anatase TiO_2 single crystals with a large percentage of reactive facets. Nature. 2008; 453: 638–641. doi: 10.1038/nature06964 PMID: 18509440
20. Hu LH, Peng Q, Li YD. Selective synthesis of Co_3O_4 nanocrystal with different shape and crystal plane effect on catalytic property for methane combustion. J. Am. Chem. Soc. 2008; 130: 16136–16137. doi: 10.1021/ja806400e PMID: 18998643
21. Som S, Kumar V, Kumar V, Gohain M, Pandey A, Duvenhage MM, et al. Dopant distribution and influence of sonication temperature on the pure red light emission of mixed oxide phosphor for solid state lighting. Ultrason. Sonochem. 2016; 28: 79–89. doi: 10.1016/j.ultsonch.2015.07.003 PMID: 26384886
22. Wu Y. Nano-crystalline oxide semiconductors for dye-sensitized solar cells. In: Yang P, editor. The Chemistry of nanostructured materials. World Scientific Publishing Company Pvt. Ltd.; 2011. 127–173.
23. Ong KP, Fan X, Subedi A, Sullivan MB, Singh DJ. Transparent conducting properties of $SrSnO_3$ and $ZnSnO_3$, APL Mater. 2015; 3: 062505 (8pp.).
24. Mali SS, Shim CS, Hong CK. Highly porous Zinc Stannate (Zn_2SnO_4) nanofibers scaffold photoelectrodes for efficient methyl ammonium halide perovskite solar cells. Sci. Rep. 2015; 5: 11424 (14pp.). doi: 10.1038/srep11424 PMID: 26094863
25. Cai P, Ma DK, Liu QC, Zhou SM, Chen W, Huang SM. J. Mater. Chem. A. 2013; 1: 5217–5223.
26. Zeng J, Xin M, Li K, Wang H, Yan H, Zhang W. Transformation process and photocatalytic activities of hydrothermally synthesized Zn_2SnO_4 nanocrystals. J. Phys. Chem. C. 2008; 112: 4159-41-67.
27. Kumar AA, Kumar A, Quamara JK, Dillip GR, Joo SW, Kumar J. Fe(III) induced structural, optical, and dielectric behavior of cetyltrimethyl ammonium bromide stabilized strontium stannate nanoparticles synthesized by a facile wet chemistry route, RSC Adv. 2015; 5: 17202–17209.
28. Kumar A, Shrivastava VP, Maurya D, Park SS, Kim JY, Jang BY, et al. Large red emission efficiency of europium activated, bismuth sensitized fine-grain calcium molybdate phosphors. Adv. Chem. Lett. 2015; 2: 3–8.
29. Errandonea D, Manjon FJ. Pressure effects on the structural and electronic properties of ABX_4 scintillating crystals. Prog. Mater. Sci. 2008; 53: 711–773.
30. Kumar A, Thota S, Sivakumar S, Priya S, Kumar J. Sol-gel synthesis and optical behavior of Mg-Ce-O nanocrystals. J. Sol-Gel. Sci. Technol. 2013; 68: 46–53.
31. Som S, Sharma SK. Eu^{3+}/Tb^{3+}-codoped Y_2O_3 nanophosphors: Rietveld refinement, bandgap and photoluminescence optimization. J. Phys. D. 2012; 45: 415102.
32. Som S, Kunti AK, Kumar V, Kumar V, Dutta S, Chowdhury M, et al. Defect correlated fluorescent quenching and electron phonon coupling in the spectral transition of Eu^{3+} in $CaTiO_3$ for red emission in display application. J. Appl. Phys. 2014; 115: 193101.

33. Som S, Mitra P, Kumar V, Kumar V, Terblans JJ, Swart HC, et. al. The energy transfer phenomena and colour tunability in $Y_2O_2S:Eu^{3+}/Dy^{3+}$ micro-fibers for white emission in solid state lighting applications. Dalton T. 2014; 43: 9860–9871.

34. Young DL, Moutinho H, Yan Y, Coutts TJ. Growth and characterization of radio frequency magnetron sputter-deposited zinc stannate, Zn_2SnO_4 thin films. J. Appl. Phys. 2002; 92: 310–319.

35. Zhu H, Yang D, Yu G, Zhang H, Jin D, Yao K. Hydrothermal synthesis of Zn_2SnO_4 nanorods in the diameter regime of sub-5 nm and their properties. J. Phys. Chem. B. 2006; 110: 7631–7634. PMID: 16610852

36. Zeng J, Xin M, Li K, Wang H, Yan H, Zhang W. Transformation process and photocatalytic activities of hydrothermally synthesized Zn_2SnO_4 nanocrystals, J. Phys. Chem. C. 2008; 112: 4159–4167.

37. Tan B, Toman E, Li Y, Wu Y. Zinc Stannate (Zn_2SnO_4) dye-sensitized solar cells. J. Am. Chem. Soc. 2007; 129: 4162–4163. PMID: 17371032

38. Alpuche-Aviles MA, Wu Y. Photoelectrochemical study of the band structure of Zn_2SnO_4 prepared by the hydrothermal method. J. Am. Chem. Soc. 2009; 131: 3216–3224. doi: 10.1021/ja806719x PMID: 19219993

39. Zhu H, Yang D, Yu G, Zhang H, Jin D, Yao K. Hydrothermal synthesis of Zn_2SnO_4 nanorods in the diameter regime of sub-5 nm and their properties. J. Phys Chem B. 2006; 110: 7631–7634. PMID: 16610852

40. Xu J, Jia X, Lou X, Shen J. One-step hydrothermal synthesis and gas sensing property of $ZnSnO_3$ microparticles. Solid-State Electron. 2006; 50: 504–507.

41. Miyauchi M, Liu Z, Zhao ZG, Anandan S, Hara K. Single crystalline zinc stannate nanoparticles for efficient photo-electrochemical devices. Chem. Commun. 2010; 46: 1529–1531.

42. Sevik C, Bulutay C. High dielectric constant and wide band gap inverse silver oxide phases of the ordered ternary alloys of SiO_2, GeO_2, and SnO_2. Phys. Rev. B. 2006; 74: 193–201.

43. Lan JL, Wang YY, Wan CC, Wei TC, Feng HP, Peng C, et al. The simple and easy way to manufacture counter electrode for dye-sensitized solar cells. Curr. Appl. Phys. 2010; 10: S168–S171.